Environmental Science & Technology

pubs.acs.org/est

Article

Eutrophication-Driven Changes in Plankton Trophic Interactions: Insights from Trade-Offs in Functional Traits

Xiaoxiao Li, Zhihao Xu,* Sibo Zhang, Weilun Gao, Qian Dong, Fen Guo, Zhenchang Zhu, Wei Yang, and Zhifeng Yang*

Cite This: https://doi.org/10.1021/acs.est.4c08067

Read Online

ACCESS | Metrics & More | Article Recommendations | Supporting Information

ABSTRACT: Understanding how plankton trophic interactions, particularly phytoplankton nutrient uptake and zooplankton grazing, respond to eutrophication is important for maintaining aquatic ecosystem functions and developing effective mitigation strategies. Phytoplankton exhibit trade-offs in functional traits between growth rate and antipredation defense, thereby regulating these trophic interactions. However, the combined effects of eutrophication and such trait-based regulation on plankton communities and interactions remain poorly understood. In the present study, we investigated these effects by integrating trait-based mechanistic modeling and field observations in China's eutrophic Pearl River Estuary. Our model predicted that the species with the weakest defensive capacities dominated under nutrient-poor conditions. As eutrophication increased, a concave growth−defense trade-off favored species with high growth rates and strong defense capacities, whereas a convex trade-off curve favored species that were either the least or the most well-defended. High grazing pressure accelerated these shifts. In the estuary, similar patterns emerged in the relative abundance of different phytoplankton species along a gradient of the nitrogen to phosphorus ratio (N:P), indicating changes from high nutrient uptake and low grazing under oligotrophic conditions to eutrophic conditions, in which some phytoplankton face considerable grazing pressure despite high nutrient uptake, whereas others grow slowly with less grazing pressure. These results enhance our understanding of trait-based plankton interactions in eutrophic bodies of water and provide support for more effective conservation and management strategies.

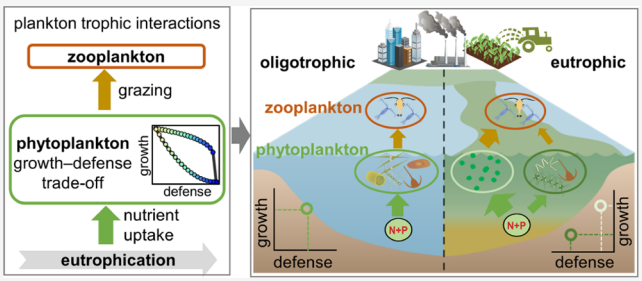

KEYWORDS: *eutrophication, trophic interaction, functional trait, growth−defense trade-off, estuary, N:P ratio, nutrient uptake, zooplankton grazing, resource use efficiency*

1. INTRODUCTION

Human activities increase nitrogen (N) and phosphorus (P) pollution, leading to eutrophication in aquatic ecosystems.[1,2] Eutrophication fundamentally alters plankton community dynamics by influencing phytoplankton nutrient uptake and subsequent consumption by zooplankton.[3] These changes degrade water quality, threaten the stability of pelagic food webs, and undermine the ecological functioning and biodiversity of aquatic ecosystems.[4,5] Understanding these interactions is critical for developing effective management and mitigation strategies to preserve the health and resilience of aquatic environments in the face of increasing nutrient pollution.

Changes in nutrient loads and ratios (e.g., N:P) can be attributed to the effects of bottom-up forces on the phytoplankton community, thereby affecting species composition, diversity, biomass, and particularly the efficiency of nutrient utilization.[6,7] This efficiency, known as the resource use efficiency (*RUE*), is defined as the amount of biomass produced per unit of supplied resource and indicates how effectively phytoplankton utilize the available nutrients.[8,9] Abrupt shifts from low to high *RUE* values have been observed for N in phytoplankton with increasing eutrophication levels.[10] However, such shifts were not consistently observed, likely due to differences among studies in the ecosystem type, phytoplankton species composition, and the degree of eutrophication.[11,12] Under conditions of highly imbalanced N and P, phytoplankton *RUE* for N often decreases with an increasing N:P ratio, whereas phytoplankton *RUE* for P increases, although these trends are also influenced by species richness.[11,13]

During zooplankton grazing on phytoplankton, studies in oligotrophic lakes have shown that zooplankton biomass scales proportionally with the phytoplankton biomass, resulting in a constant *RUE* of the zooplankton (i.e., a stable biomass ratio

Received: August 4, 2024
Revised: December 3, 2024
Accepted: December 3, 2024

between the zooplankton and phytoplankton).[14] Conversely, in eutrophic lakes, the *RUE* of the zooplankton grazing on phytoplankton decreased with increasing eutrophication.[10,15] Such a reduction may result from several mechanisms, such as increased mortality of zooplankton due to predation by planktivores or strengthened antipredation defense mechanisms of the phytoplankton species, of which the latter has been extensively documented in trait-based studies.[16−19] These defenses are evolutionary strategies developed to mitigate herbivory, including structural defenses, such as thorns and spines that are difficult to consume, and chemical defenses, such as toxic substances.[20]

However, developing these defenses requires energy, and thus often incurs physiological costs, such as decreased growth rates or reduced competitive abilities, which highlights a fundamental trade-off between growth and defense.[21] Such a growth−defense trade-off by phytoplankton has been well-documented in both natural ecosystems and laboratory experiments. For example, a negative relationship between phytoplankton's growth and their defensive strength (the inverse of edibility) was observed for the consumption of *Daphnia* in Lake Constance.[22] In addition, a trade-off between growth and toxin production to defend against copepod grazing was demonstrated for *Alexandrium minutum* in a laboratory experiment.[23] A recent experiment showed that diatoms typically exhibit a 10% decrease in growth rate alongside a 16% increase in cellular biogenic silica. This silica increase is associated with an 11% reduction in grazing mortality caused by small copepods.[24]

The growth−defense trade-off further complicates interactions within the nutrient−phytoplankton−zooplankton system by altering phytoplankton investment in growth versus defenses against zooplankton predation (Figure 1). Recent theoretical studies have highlighted the critical importance of the growth−defense trade-off in shaping the interplay between top-down and bottom-up controls of plankton communities, thereby affecting the overall community structure.[25−27] For instance, the growth−defense trade-off governs how the phytoplankton community composition responds to seasonally varying zooplankton grazing pressure.[22] However, it remains unclear how increasing eutrophication will affect the growth−defense trade-off and thus, how it will shape the trophic interactions within the nutrient−phytoplankton−zooplankton system. Such research would contribute to predicting how complex trophic interactions will respond to environmental stress and the trait-based mechanisms involved in that response. It would also contribute to trait-based adaptive management and conservation of eutrophic aquatic ecosystems.

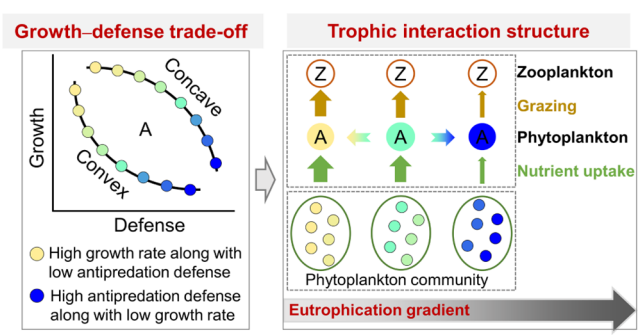

Figure 1. Schematic diagrams of how the growth−defense trade-offs among phytoplankton species and the eutrophication gradient alter the structures of plankton trophic interactions and phytoplankton community compositions. Phytoplankton species may exhibit concave or convex shapes in their growth−defense trade-off. A denotes autotrophs (phytoplankton) and Z denotes zooplankton. The different colors for circle A represent different phytoplankton species shown in the trade-off curves, with species exhibiting a unique combination of defense and growth traits.

In this study, we combined trait-based mechanistic modeling and field observations in a eutrophic estuary. Figure S1 illustrates the connections between the two approaches. The trait-based plankton model we developed includes a range of phytoplankton species that exhibit different trade-offs between growth and defense, along with a zooplankton group that grazes on these phytoplankton. Using this model, we investigated which phytoplankton species persist and dominate by adopting specific growth-defense trait combinations across a gradient of eutrophication and varying levels of zooplankton grazing pressure. In addition, we conducted field observations in the eutrophic Pearl River Estuary in China, where human activities have severely increased N loads, and measures to mitigate eutrophication have typically reduced P more than N, resulting in a shift toward higher N:P ratios and consequent eutrophication stress.[28] We investigated the abundance and biomass of phytoplankton and zooplankton, the *RUE*s of phytoplankton for N and P, and the *RUE* of zooplankton grazing on phytoplankton across the gradient of N:P ratios. We then quantified the maximum growth rates and defense capacities of all collected phytoplankton species to evaluate their growth−defense trade-offs, examining how these trade-offs vary under low and high N:P ratios. Finally, we compared the model-predicted patterns of species persistence and community structure with field observations in the Pearl River Estuary, thereby enhancing our understanding of trait-based mechanistic plankton interactions in eutrophic estuaries.

2. MATERIALS AND METHODS

2.1. Trait-Based Plankton Model. *2.1.1. Model Structure.* We developed a trait-based plankton model (for 20 phytoplankton species and 1 zooplankton group) to explore how the eutrophication gradient and the different growth and antipredation defense strategies of the phytoplankton species influenced their community composition and trophic interactions with zooplankton. In this model, phytoplankton species face a trade-off between maximizing their growth rate and their defense capacity against zooplankton grazing pressure.[21] The biomass dynamics of these phytoplankton species are modeled as described elsewhere:[22]

$$\frac{dA_i}{dt} = \left(r_i \frac{R}{K + R} - \frac{G(1 - \delta_i)Z}{H + \sum_{i=1}^{n} A_i} - m_A \right) A_i \quad (1)$$

where A_i represents the biomass of autotrophic (phytoplankton) species i, r_i is the maximum growth rate of phytoplankton species i, K is the half-saturation constant for nutrient uptake, G is the maximum grazing rate of zooplankton, δ_i is the defense capacity of phytoplankton species i against zooplankton, which requires a trade-off with r_i, Z is the zooplankton biomass, H is the half-saturation constant of zooplankton for phytoplankton ingestion, and m_A is the natural mortality of phytoplankton independent of the phytoplankton species identity. R is the available nutrient from the assumed total fixed nutrient pool (T_R), and is expressed as

https://doi.org/10.1021/acs.est.4c08067
Environ. Sci. Technol. XXXX, XXX, XXX−XXX

$$R = T_R - \sum_{i=1}^{n} A_i - \frac{1}{\varepsilon} Z \tag{2}$$

where n represents the number of phytoplankton species (n = 20), and ε denotes the conversion efficiency of zooplankton grazing on phytoplankton. T_R can serve as an indicator of the eutrophication gradient, as it reflects the maximum availability of nutrients.

The biomass dynamics of the zooplankton group can be expressed as

$$\frac{dZ}{dt} = \left(\varepsilon \frac{G \sum_{i=1}^{n} [(1 - \delta_i) A_i]}{H + \sum_{i=1}^{n} A_i} - m_Z \right) Z \tag{3}$$

where m_Z is the mortality of zooplankton.

2.1.2. Numerical Simulation. Phytoplankton species can exhibit varied curves for their growth−defense trade-off, such as linear or concave or convex, where the curve represents the boundary of feasible trait combinations.[25,29] These distinct shapes reflect differences among species in the costs of trait adjustments under constraints such as energetic, nutrient, or physiological limitations in response to changing environmental conditions.[21] A convex growth−defense trade-off curve indicates a significantly higher antipredation cost compared to a concave curve. The shape of these trade-off curves has been shown to influence the potential for species coexistence and the dynamics of community biomass.[26] Moreover, the zooplankton grazing pressure influences the selection of strategies among phytoplankton species. Thus, we performed numerical simulations of (1) a continuous nutrient gradient, (2) low versus high zooplankton grazing pressures, and (3) concave or convex growth−defense trade-off curves.

Specifically, we modeled a continuous gradient of the fixed nutrient pool (T_R) ranging from 10 to 10,000 to indicate the eutrophication gradient. For other parameter values, see Table S1. The mortality of zooplankton, denoted by m_Z, includes losses due to predation by organisms at higher trophic levels and nonpredatory causes such as insufficient nutrition, environmental stress from physical or chemical factors, and physiological decline associated with aging.[30] This mortality rate, in turn, reflects the intensity of grazing pressure that zooplankton exerts on phytoplankton. Based on previous modeling,[22] we assumed m_Z = 0.05 to represent a high level of grazing pressure on phytoplankton by zooplankton and m_Z = 0.15 to represent a lower level of grazing pressure (Table S1). For the growth−defense trade-offs, we used three parameters to define their shape:

$$r_i = b(1 - \delta_i)^a + c \tag{4}$$

where a controls the shape of the trade-off: for $a < 1$, the curve is concave and $a > 1$, convex; b represents the slope of the curve; and c gives the maximum growth rate of the most defended species ($\delta_i = 1$). We assumed that a = 0.2, b = 1.6, and c = 0.8 for a concave curve and a = 2.8, b = 1.6, and c = 0.8 for a convex curve (Figure S2).

In each simulation, we assigned the defense traits of the 20 phytoplankton species by sampling equally spaced values along the entire defense trait axis (0 to 1). The initial biomass for each phytoplankton species was assigned randomly within a range of 0.1 to 1.0. For zooplankton, the range was 1 to 40 based on the relative biomass structure from our field measurements in the estuary. Simulations were conducted over 10,000 time-steps with a step size of 0.1 to ensure that the simulations reached stationary equilibria. We used the average relative biomass of the phytoplankton species over the final 2000 time-steps to represent the characteristics of the different equilibria. Species were assumed to be extinct once their biomass decreased below 10^{-6}.[31] All numerical simulations were run in MATLAB, version 2018b, using solver ode45 with absolute and relative error tolerances of 10^{-8} and 10^{-10}, respectively.

2.2. Case Study. *2.2.1. Study Site and Field Sampling.* The Pearl River is China's second-largest river in terms of freshwater discharge (i.e., approximately 3.3×10^{11} m^3 yr^{-1}), with a drainage area of 4.5×10^5 km^2. Lingdingyang Bay, the largest subestuary of the Pearl River, receives about 53% of the river's total discharge and faces significant eutrophication challenges due to its substantial inflow, proximity to densely populated urban areas, and semiclosed topography.[32] Therefore, we chose Lingdingyang bay as the study region.

Field sampling was conducted during cruises in April 2023 and September 2023. We established 12 stations in April and 13 stations in September that were distributed uniformly from the upper river channel to the coastal waters (Figure S3). The total area represented by the sampling stations was approximately 1504 km^2 (Figure S3). The maximum straight-line distance from the upper river to the lower estuary is 64 km in April and 96 km in September. The distance between adjacent pairs of sampling stations ranged from 6.3 km to 19.3 km in April and from 7.4 km to 18.3 km in September. At each sampling station, we investigated the physicochemical characteristics of the surface water and collected samples from near-surface depths (both at 0.8 to 1.0 m). Water temperature (*water T*, °C), dissolved oxygen (*DO*, mg/L), salinity (‰), and pH were measured *in situ* using a ProPlus YSI6600 multiparameter probe (YSI, Beijing, China). The water depth was measured *in situ* with a handheld depth sounder (SM-5A, Speedtech, River Falls, WI, USA). After filtration of each raw water sample through a 45 mm Whatman glass-fiber filter, we measured the chlorophyll *a* content (Chl *a*, mg/L) spectrophotometrically.[33] In addition, 2-L water samples were stored in polyethylene bottles and then transported to the laboratory for measurement of total nitrogen (*TN*, mg/L), ammonia nitrogen (NH_3−N, mg/L), nitrite nitrogen (NO_2−N, mg/L), nitrate nitrogen (NO_3−N, mg/L), total phosphorus (*TP*, mg/L), and dissolved phosphate (PO_4−P, mg/L) according to the methods defined in the national standard of China (GB/T 11893−1989).[34] The total concentration of NH_3−N, NO_2−N, and NO_3−N equaled the concentration of dissolved inorganic nitrogen (*DIN*, mg/L). The ratio of nitrogen to phosphorus (N:P) was calculated as the ratio of *DIN* to PO_4−P. For the temporal and spatial distributions of these water physicochemical factors, see Figure S4.

Phytoplankton and zooplankton were each collected in three parallel samples at each station. Phytoplankton was sampled using a Plankton Net III (77-μm mesh size, 140 cm long, 37 cm mouth diameter). Small and large zooplankton were sampled using a Plankton Net II (160-μm mesh size, 140 cm long, 32 cm mouth diameter) and Plankton Net I (505-μm mesh size, 145 cm long, 50 cm mouth diameter), respectively. Sampling was conducted by towing the nets vertically from 0.5 m above the bottom to the surface at a constant speed of 0.5 m/s.[35] A heavy hammer that weighed 20 to 40 kg was attached during sampling to ensure the nets reached the bottom. We preserved the samples in Lugol's solution, transferred them to

https://doi.org/10.1021/acs.est.4c08067
Environ. Sci. Technol. XXXX, XXX, XXX−XXX

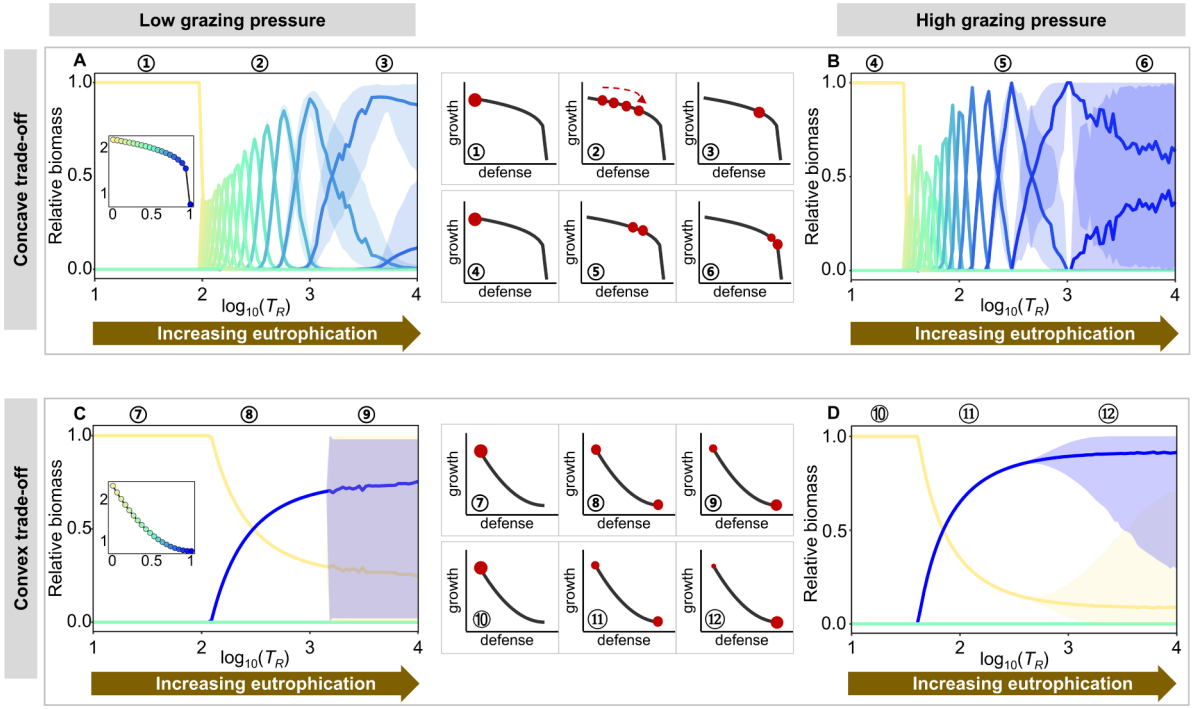

Figure 2. Biomass dynamics of phytoplankton species across the eutrophication gradient indicated by the total fixed nutrient pool (T_R) (Table S1), with the dynamics derived from the trait-based plankton model. This model incorporates 20 phytoplankton species and a single zooplankton group. In the top panel (A, B), the 20 phytoplankton species were characterized by distinct growth and defense strategies from the concave trade-off curve (indicated by different colors) and are shown under two different levels of grazing pressure: low pressure (left, with a zooplankton mortality rate of $m_Z = 0.15$) and high pressure (right, with $m_Z = 0.05$). The middle of this panel (inset graphs 1 to 6) highlights the strategy of the dominant species throughout the eutrophication gradient. The bottom panel (C, D) modeled the 20 phytoplankton species following a convex trade-off curve, with a similar analysis. The lines represent the average relative species biomass over the final 2000 iterations of 10,000 time-steps. The shaded areas above and below these lines denote the maximum and minimum relative biomass values for the species observed during these last 2000 steps, indicating the presence of biomass oscillations (Figure S6).

the laboratory, and identified the taxa under an Olympus CX31 optical microscope (Olympus, Tokyo, Japan). All species were identified to the class, genus, or species level. We used the geometric shape closest to the actual cell shape to calculate the mean cell biovolume, which we then transformed into a wet weight to estimate phytoplankton biomass.[36] For zooplankton, if a species was captured by both nets (II and I) at the same sampling time and location, its abundance was calculated by dividing the total number of sampled individuals by the total filtered water volume from both nets combined. If a species was only collected from one net, its abundance was calculated using data solely from that net. The zooplankton biomass for each sample was then calculated by multiplying the abundance of each taxon by its taxon-specific average wet weight and then summing these values for the entire sample.[30]

We investigated the dominance of each phytoplankton species in each sampling period, which was calculated as follows:

$$Y_i = \frac{n_i}{N} f_i \tag{5}$$

where Y_i is the relative dominance of species i in a given sampling period, n_j is the number of individuals of species i, N is the total number of individuals sampled in this period, and f_i is the percentage of all sampling sites where species i was found. When $Y_i \geq 0.02$, the species is regarded as being one of the dominant species.[37]

2.2.2. Phytoplankton and Zooplankton RUE. *RUE* is often defined as the proportion of available resources incorporated into species biomass.[9] *DIN* and PO_4−P were used as measures of the available resources for phytoplankton *RUE*.[38] This is mainly because N and P, which are the most bioavailable substrates of *DIN* and PO_4−P, are the major nutrient sources for phytoplankton in aquatic ecosystems.[15] In this study, we calculated several aspects of phytoplankton *RUE*. Specifically, we calculated phytoplankton *RUE* with respect to Chl *a* using *DIN* and PO_4−P:

$$RUE_{\text{Chl–N}} = \log_{10}(\text{Chl } a\text{: } DIN) \tag{6}$$

$$RUE_{\text{Chl–P}} = \log_{10}(\text{Chl } a\text{: } PO_4 - P) \tag{7}$$

The calculations of phytoplankton *RUE* with respect to phytoplankton biomass for utilizing *DIN* and PO_4−P were expressed as follows:

$$RUE_{\text{phy–N}} = \log_{10}(\text{phytoplankton biomass: } DIN) \tag{8}$$

$$RUE_{\text{phy–P}} = \log_{10}(\text{phytoplankton biomass: } PO_4 - P) \tag{9}$$

For zooplankton, *RUE* measures how efficiently they convert phytoplankton biomass into their own biomass, which is expressed as

$$RUE_{\text{zoo}} = \log_{10}(\text{zooplankton biomass : phytoplankton biomass}) \tag{10}$$

2.2.3. Phytoplankton Functional Traits. We collected 68 phytoplankton species (Table S2) across 24 orders, 5 classes,

https://doi.org/10.1021/acs.est.4c08067
Environ. Sci. Technol. XXXX, XXX, XXX−XXX

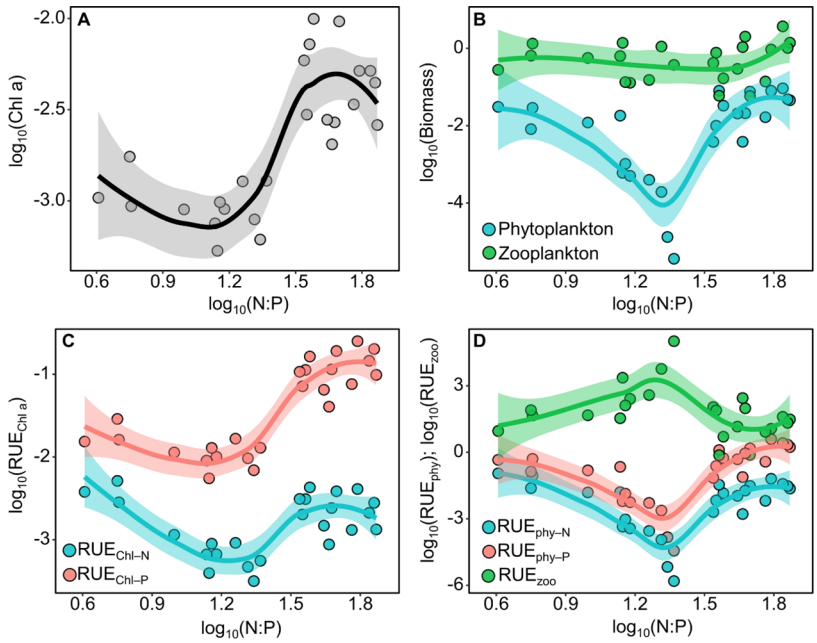

Figure 3. Chlorophyll *a* (Chl *a*, mg/L) (A) concentrations and (C) resource-use efficiency (*RUE*) along the gradient of N:P ratios, calculated as the *DIN*:PO_4−P ratio, in the Pearl River Estuary. (B) Biomass (mg/L) and (D) the *RUE* of phytoplankton and zooplankton along the N:P gradient in the estuary. Nonlinear curves were fitted using the locally estimated scatterplot smoothing method.

and 5 phyla (Figure S5). The cell biovolume of these species differed widely, with values ranging from 200 to 7.6×10^7 μm^3 $cell^{-1}$, which agrees with previously reported ranges.[39,40] The maximum growth rates (r, d^{-1}) indicated the growth potential of phytoplankton under optimal light and nutrient availability conditions.[41] The interspecific variability of r is known to be influenced by the cell biovolume (V), with the smallest cells having the highest growth rates. This advantage is attributed to the catalytic efficiency of smaller cells, which enables them to outcompete larger counterparts.[40] We initially sourced r values from the literature[39,42−44] based on species identity and an assumed temperature of 20 °C, which represents the annual average temperature of our study region. This approach gave us r values for 70% of the collected species, resulting in the equation $r = 3.9V^{-0.08}$ ($R^2 = 0.58$, $p < 0.001$). We used this equation to estimate r for the remaining species.

To assess the defense capacity of phytoplankton against zooplankton grazing, we developed a composite defense trait modified from the traits defined in previous research.[27,45] This evaluation considered each species' escape ability, mucus or toxin production, and defensive structures (i.e., setae and spicules, degree of silicification) to prevent zooplankton grazing, and we assigned their scores as follows: (i) motility (0, without motility; 0.5, floating; 0.75, gliding; 1.0, swimming); (2) capacity to produce mucus or toxins (0, no; 1, yes); (3) the presence of setae and spicules, which enhance buoyancy (0, no; 1, yes); and (4) the degree of silicification (0, slight; 0.5, medium; 1.0, heavy). The sum of these scores equaled the defense trait of each species. We then standardized the defense traits for all species to a scale ranging from 0 to 1, where 0 represents the least defended and 1 the most defended. Table S2 lists the phytoplankton species and their trait values.

2.2.4. Data Analysis. Statistical analyses were performed using the R software (version 4.0.2).[46] We investigated the changes of Chl *a*, species biomass, and the different aspects of *RUE* across the N:P gradient by applying locally estimated scatterplot smoothing to illustrate general trends. The parameters of the growth−defense trade-off curve (*a*, *b*, and *c*, eq 4) for collected phytoplankton species in the estuary were estimated through iterative nonlinear curve fitting in regression analysis using the *nlsLM* function from the minpack.lm package in R.[47] We also used the Spearman rank correlation to examine the correlation between the species' maximum growth rates and their defense capacities. In addition, we employed a Mantel test using the *mantel* function from the R Vegan package[48] to examine the associations between species biomass, phytoplankton growth, defense traits, and *RUE*s in relation to the water physicochemical factors. Along with the Mantel test, we used Pearson's correlation coefficient to represent the strength of the relationships among the water physicochemical factors (with significance at $p < 0.05$). Distance matrices for water physicochemical factors and plankton properties were calculated using Euclidean and Bray−Curtis distances, respectively.

3. RESULTS

3.1. Predictions from the Trait-Based Plankton Model. Our trait-based plankton model revealed a variety of equilibrium states along the eutrophication gradient indicated by T_R in terms of species persistence and relative biomass within the phytoplankton community (Figure 2). Under conditions of a concave growth−defense trade-off combined with low zooplankton grazing pressure, the model predicted that only the species with the least defense capacity but the highest growth rate survived at low T_R (Figure 2A). This is because the zooplankton could not survive under a scarcity of nutrients (Figure S6). As T_R increased, there was a gradual transition toward species with a higher defense and thereby a lower growth rate becoming dominant (Figure 2A). Increased grazing pressure accelerated this shift, resulting in dominance by species with enhanced defense and reduced growth at a given T_R (Figure 2B) compared to scenarios with lower grazing

https://doi.org/10.1021/acs.est.4c08067
Environ. Sci. Technol. XXXX, XXX, XXX−XXX

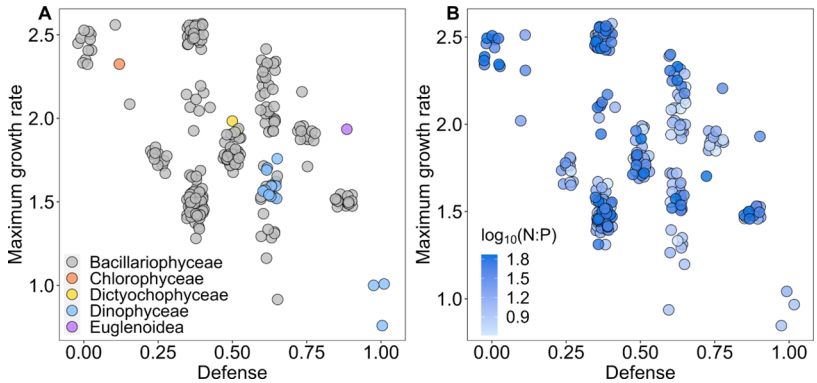

Figure 4. Phytoplankton growth−defense trade-offs for the (A) five phyla and (B) for the logarithmic N:P ratio of the sampling site where each species was collected. Random variations (±0.03 along the *x*-axis; ±0.05 along the *y*-axis) were introduced to minimize overlap among the data points. Species' growth ability was represented by their maximum growth rate (d^{-1}) as a function of their cell volume according to an allometric scaling law. The defense traits of all species were standardized to a scale from 0 to 1, with 0 representing the least defended and 1 the most defended. These defense values were calculated by accounting for a species' escape ability, mucus or toxin production, and structural features such as setae and silicification to prevent zooplankton grazing (Table S2).

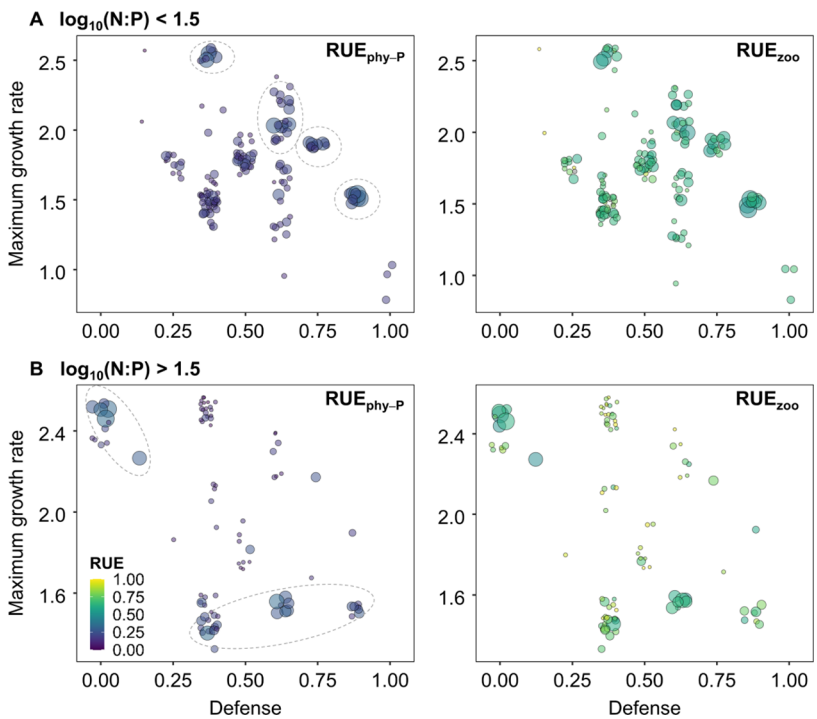

Figure 5. Phytoplankton species growth−defense trade-off patterns within two subgroups based on the logarithmic N:P ratios of their sampling sites: (A) below 1.5 and (B) higher than 1.5. Random variations (±0.03 along the *x*-axis; ± 0.05 along the *y*-axis) were introduced to reduce overlap among data points. Circles are scaled by the relative biomass for the species within each subgroup. Colors denote the standardized values of RUE_{phy-P} in the left panels and RUE_{zoo} in the right panels for each subgroup. Similar patterns in standardized values of RUE_{phy-N} were observed (Figure S9). Species' growth ability was represented by their maximum growth rate (d^{-1}) dependent on their cell volume according to the allometric scaling law. The defense traits of all species were standardized to a scale from 0 to 1, with 0 representing the least defended and 1 the most defended. These defense values were calculated by accounting for species' escape ability, mucus or toxin production, and structural features such as setae and silicification to prevent zooplankton grazing (Table S2).

pressure (Figure 2A). Conversely, convex growth−defense trade-off led to a survival and dominance shift from species with high growth rates but no defenses to species that were either the most heavily defended or least defended as T_R increased (Figure 2C). Elevated zooplankton grazing pressure accelerated this shift, emphasizing the dominance of the most defended species at higher T_R levels (Figure 2D).

Increasing T_R typically intensified oscillations of the biomass dynamics of the persisting species (shaded regions in Figure 2). Once these oscillations emerged, phytoplankton species that persisted often displayed antiphase cycles in their biomass dynamics; that is, when one species reached its maximum biomass, another one was at its minimum level (Figure S7). Within the convex trade-off scenario, we observed temporal shifts in dominance among the oscillations in phytoplankton species' biomasses—from species with the strongest defense to those with the lowest defense—at high T_R levels (Figure S7).

3.2. Species Biomass and *RUE* Changed along the N:P Gradient in the Pearl River Estuary. Significant differences were observed in the estuary's water temperature, salinity, *DO*,

https://doi.org/10.1021/acs.est.4c08067
Environ. Sci. Technol. XXXX, XXX, XXX−XXX

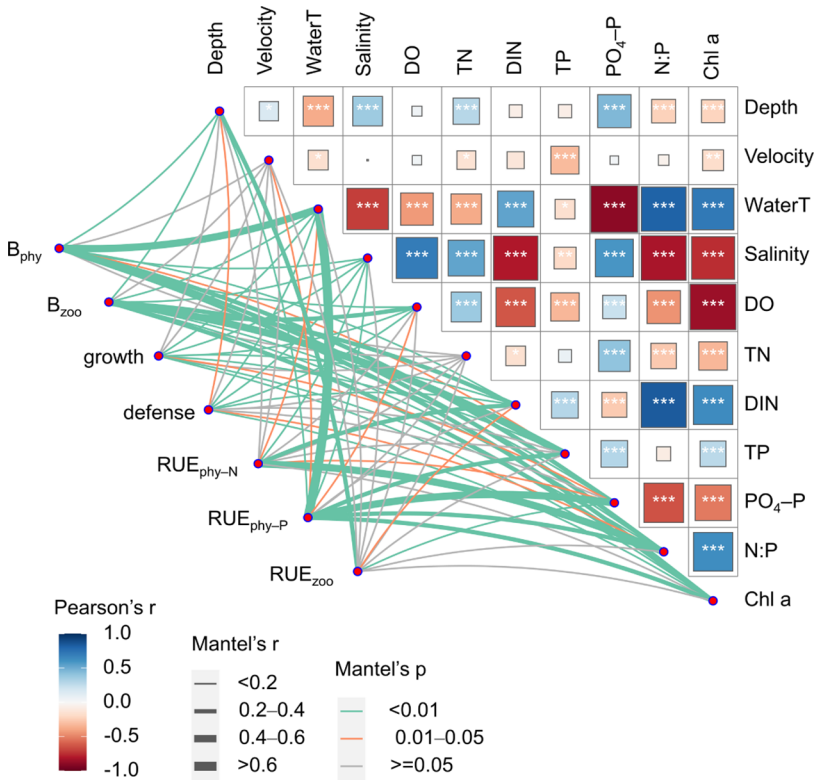

Figure 6. Pearson's correlations between water physicochemical factors and the Mantel test of species biomass, functional traits, and *RUE*s concerning these physicochemical factors in the Pearl River Estuary. B_{phy} and B_{zoo} are biomasses of phytoplankton and zooplankton, respectively. The "Materials and Methods" section defines abbreviations for physicochemical variables.

DIN, PO_4−P, N:P, and Chl *a* between the two sampling periods (Table S3). The N:P ratios and *DIN* were significantly higher in September than in April, but PO_4−P showed the opposite trend (Figure S4). The higher N:P ratios were predominantly found in the western part of the lower estuary, which was generally consistent with the distribution of *DIN* but opposite to that of PO_4−P (Figure S4). Throughout the investigation, diatoms (Bacillariophyta) accounted for 87% of the total phytoplankton species in the estuary (Table S2). *Skeletonema costatum*, *Chaetoceros curvisetus*, *Chaetoceros lorenzianus*, and *Ditylum brightwellii* were dominant species in April. *Aulacoseira granulata* and *Coscinodiscus* sp. were dominant in September (Table S4).

The Chl *a* concentration and phytoplankton biomass showed similar trends along the N:P gradient, initially decreasing and then increasing (Figure 3A,B). Zooplankton biomass remained relatively stable throughout the N:P gradient, with a slight increase at higher N:P ratios, and was consistently higher than phytoplankton biomass (Figure 3B). The *RUE* of Chl *a* concerning nitrogen (RUE_{Chl-N}) and phosphorus (RUE_{Chl-P}), and the *RUE* of phytoplankton for nitrogen and phosphorus (RUE_{phy-N}, RUE_{phy-P}), generally showed consistent trends across the N:P gradient (Figures 3C,D), although the gap between the two types of *RUE* was much larger for Chl *a*. The lowest *RUE* values occurred around a $\log_{10}$(N:P) ratio of 1.2 to 1.5. Conversely, zooplankton *RUE* (RUE_{zoo}) showed the opposite trend. RUE_{zoo} was generally higher than both RUE_{phy-N} and RUE_{phy-P}, with the difference being particularly noticeable around a $\log_{10}$(N:P) ratio of 1.2 to 1.5, implying a pronounced zooplankton grazing pressure coupled with a limited nutrient uptake by phytoplankton. Notably, a $\log_{10}$(N:P) ratio between 1.2 and 1.5 appeared to be a critical point where the trends of phytoplankton and zooplankton *RUE* changed direction.

3.3. Phytoplankton Growth−Defense Trade-Offs and Their Impacts on Species Biomass and *RUE* in the Pearl River Estuary. Our analysis of the 68 phytoplankton species collected from the estuary revealed a concave growth−defense trade-off, with parameters $a = 0.26$ (SE = 0.09, $p < 0.001$), $b = 1.07$ (SE = 0.21, $p < 0.001$), and $c = 0.95$ (SE = 0.21, $p < 0.001$) for eq 4 (Figure 4A). A higher capacity for defense against grazing was correlated with a reduced maximum growth rate, and vice versa (Spearman rank correlation coefficient $\rho = -0.18$, $p = 0.006$). For instance, *Cyclotella* sp. exhibited the highest maximum growth rate, at 2.55 d^{-1}, with a relatively low defense rating of 0.125 (standardized value) (Figure 4A). Conversely, *Tripos macroceros* demonstrated the lowest maximum growth rate, at 0.80 d^{-1}, but had the highest defense rating of 1. Further investigation into the growth−defense trade-off along the N:P gradient revealed potentially different patterns of growth and defense combinations (Figure 4B). Under low N:P conditions, the nonlinear least-squares analysis yielded parameter estimates for the growth−defense trade-off, with values in eq 4 of $a = 0.07$ (SE = 0.07, $p = 0.34$), $b = 0.89$ (SE = 0.19, $p < 0.001$), and $c = 0.93$ (SE = 0.19, $p < 0.001$), suggesting a potential concave trade-off (Figure S8A). In contrast, under high N:P conditions, parameter estimates were $a = 1.84$ (SE = 0.85, $p < 0.001$), $b = 0.74$ (SE = 0.17, $p < 0.001$), and $c = 1.66$ (SE = 0.15, $p < 0.001$), suggesting a potential convex trade-off (Figure S8B).

We further analyzed the relationships between phytoplankton species trade-offs and a suite of ecological metrics, including the relative phytoplankton biomass, RUE_{phy-P}, RUE_{phy-N}, and RUE_{zoo} under low and high N:P ratios (Figure

https://doi.org/10.1021/acs.est.4c08067
Environ. Sci. Technol. XXXX, XXX, XXX−XXX

5). Since zooplankton biomass and RUE were higher than the corresponding values for phytoplankton (Figures 3), we compared field observations (Figure 5) with model predictions under high grazing pressure (Figure 2B,D). Although the patterns shown in Figure 5 were not exact duplicates of the model predictions, the structure of the phytoplankton community at $\log_{10}$(N:P) < 1.5 resembled scenario 5 in Figure 2B, and for $\log_{10}$(N:P) > 1.5, it resembled scenario 11 in Figure 2D. When the $\log_{10}$(N:P) ratio was less than 1.5, the dominant phytoplankton species exhibited a broad spectrum of growth and defense strategies, reflecting a diverse ecological adaptation to the available resources. Specifically, these species either exhibited a higher growth rate with a lower defense capacity, high levels of both growth and defense capacities, or a high defense level at the expense of a lower growth rate (see dashed circles in Figure 5A). Conversely, when the $\log_{10}$(N:P) ratio was greater than 1.5, we observed dominance by species that either adopted the highest growth rate along with a low defense or those that managed to maintain an intermediate to high defense while exhibiting relatively low growth rates (see dashed circles in Figure 5B).

The high variation in field observations compared to model predictions also suggests that additional abiotic and biotic factors might play a role in the regulating phytoplankton community structure. A Mantel test indicated significant correlations between the majority of the measured water physicochemical parameters—including depth, water temperature, salinity, *DO*, *DIN*, PO_4−P, and Chl *a*—and various attributes such as species biomass, growth, and defense traits, RUE_{phy-P}, and RUE_{phy-N} ($p < 0.05$, Figure 6). Specifically, water temperature and salinity emerged as two of the most influential factors, showing strong correlations with multiple variables, though in opposite directions. In particular, water temperature showed a strong positive correlation with phytoplankton biomass (Mantel's $r = 0.40$, $p < 0.001$). Water depth demonstrated a notable correlation with RUE_{phy-P} (Mantel's $r = 0.20$, $p = 0.001$). Salinity exhibited a positive correlation with defense traits (Mantel's $r = 0.19$, $p < 0.001$).

4. DISCUSSION

4.1. Generalizability and Limitations of the Trait-Based Plankton Model. Our trait-based plankton model incorporated 20 distinct phytoplankton species, differentiated by their growth rates and defense capacities, thereby allowing the prediction of changes in their relative dominance. Although species positioned along the growth−defense trade-off curve were assumed to have different fitness (i.e., their net per capita growth rate),[22] their ability to establish dominance also depended on the specific environmental context, including both biotic (grazing pressure) and abiotic (nutrient availability) factors. By simulating the trait-based plankton model under a range of eutrophication and grazing pressure levels, our model effectively illustrated how species sorting occurs and is driven by the adoption of growth and defense strategies across a broad range of both abiotic and biotic conditions. These findings expand upon previous trait-based models, which explored the growth−defense trade-off under only low and high grazing pressures[22] or which explored defense−competition trade-offs under fixed and discrete oligotrophic and eutrophic conditions.[26]

In environments with very low nutrient availability, species with a low investment in defense dominated the community, regardless of the shapes of the trade-off curves or grazing intensities (Figure 2). This suggests that nutrient-limited conditions favor *r*-strategist phytoplankton species.[49] This dominance mainly stems from the need for phytoplankton to maintain high growth rates in nutrient-scarce environments, where zooplankton struggle to survive due to inadequate energy supplies or exert very low grazing pressure due to their low biomass levels. An increase in grazing pressure at a given nutrient level promoted the dominance of better-defended species, which has been described as a shift toward antipredation mechanisms.[22] At a given level of grazing pressure, our model predicted that increasing nutrient availability would favor species with both fast growth and strong defense capacities, particularly when species incur a reduced cost for defense (a concave trade-off; Figure 2). In addition, under a convex trade-off, species with strong defenses were favored to coexist with less-defended species (Figure 2). This is generally consistent with prior research that suggested eutrophic conditions favor better-defended organisms[50,51] and that defense traits promote species coexistence in phytoplankton communities under eutrophic conditions.[26] Overall, our model predictions suggest that at lower eutrophication levels, nutrient uptake by phytoplankton and zooplankton grazing on phytoplankton is relatively high. In contrast, at higher eutrophication levels, some phytoplankton species manage rapid growth despite significant grazing pressure, whereas others exhibit slower growth but with reduced grazing pressure, indicating that alternative states occurred.

Our model predicted significant oscillations in species biomass under high nutrient availability, which agrees with the eutrophication paradox,[52] which suggests that elevated nutrient levels lead to unpredictable fluctuations in species populations. Our model further indicated that zooplankton exhibited much higher variation in biomass compared to the total phytoplankton biomass at high nutrient availability (Figure S6). Furthermore, our findings suggest that with a concave trade-off, high grazing pressure induced more pronounced oscillations in species biomass at high nutrient levels, whereas under the convex trade-off, the pattern was reversed.

Although our model effectively captures the traits of phytoplankton within a natural ecosystem, it does not fully address the broader ecological complexities. In particular, the model does not consider the functional traits of zooplankton, such as their grazing selectivity and their ability to overcome phytoplankton defenses.[53,54] The model is sufficiently generalizable to incorporate more traits and trade-offs in future applications. In addition, the model used T_R to represent different levels of nutrient availability, thereby letting us examine the general trends of how plankton interactions change along a eutrophication gradient. However, it lacks a direct connection between T_R and actual eutrophication indicators in natural environments. In addition, other environmental gradients, such as temperature and light, will also significantly influence plankton dynamics.[26] Expanding the model to include more environmental factors would improve our understanding of plankton dynamics under varying environments and support the development of more effective management strategies.

4.2. Specialty and Model Consistency of the Case Study in the Pearl River Estuary. The distinguishing nutrient condition of the estuary is its notably low concentration of P relative to N compared with other large

https://doi.org/10.1021/acs.est.4c08067
Environ. Sci. Technol. XXXX, XXX, XXX−XXX

estuaries such as those of the Mississippi, Yangtze, and Rhine Rivers.[28] Our fieldwork revealed N:P ratios ranging from 4 to 74, which fall within previously reported ranges (4.3 to 242.5),[55] suggesting that P is often the limiting nutrient for phytoplankton growth in the estuary. Instead of observing a single peak of Chl *a* or phytoplankton biomass at an optimal N:P ratio, such as the Redfield ratio (16:1),[56] our findings in the estuary reveal a more complex pattern. This suggests that plankton are influenced by a range of environmental factors beyond nutrient ratios, a common scenario in estuarine systems where environmental conditions fluctuate widely.

We observed mismatches in *RUE* between phytoplankton and zooplankton along the N:P gradient in the estuary, where increasing phytoplankton *RUE* (RUE_{phy-N} and RUE_{phy-P}) was associated with decreasing zooplankton *RUE* (RUE_{zoo}), and vice versa (Figure 3). Such mismatches have often been reported in studies on biodiversity and ecosystem functioning,[15,57] which suggests that phytoplankton species evenness is negatively correlated with phytoplankton *RUE* but positively correlated with zooplankton *RUE*. In the context of eutrophication, such mismatches are frequently attributed to the intensity of algal blooming,[58] where phytoplankton is dominated by species that are not easily consumed by herbivores or that are of lower nutritional quality.[51] This dominance reduces the efficiency with which consumers convert producer biomass into their own biomass. For instance, phytoplankton and zooplankton *RUE* were high and low, respectively, when Cyanobacteria, and especially *Microcystis* spp., dominated in nutrient-enriched lakes.[15] In the Pearl River Estuary, the relatively dominant species *S. costatum* and *C. curvisetus* (Table S4) have historically been reported as bloom-forming species;[59,60] in particular, *S. costatum* was recorded in 12 algal blooms across 24 cruises from 1985 to 2014.[61] This research showed that phytoplankton *RUE* increased as the relative abundance of *S. costatum* increased although there was substantial variability at low relative abundance levels of *S. costatum*, whereas zooplankton *RUE* decreased (Figure S10). Similarly, for *Coscinodiscus* sp., higher dominance was associated with increased phytoplankton *RUE* and decreased zooplankton *RUE* (Figure S10). This aligns well with recent research in which the relative abundance of dominant Bacillariophyta was positively correlated with phytoplankton *RUE* but negatively correlated with zooplankton *RUE*.[58]

Furthermore, we found the RUE_{zoo} was generally higher than RUE_{phy-N} and RUE_{phy-P} in the estuary, suggesting that phytoplankton species in the estuary experience relatively intense grazing pressure from zooplankton. This pattern likely results from the high biomass of zooplankton compared to the lower biomass of phytoplankton. This imbalance may disproportionately affect certain phytoplankton species, particularly those that prioritize rapid growth over defense mechanisms. Previous research has also documented significant copepod grazing pressure in the estuary, with spatially averaged impacts ranging from consumption of less than 0.3% to as much as 75% of the chlorophyll standing stock, and with impacts sometimes exceeding phytoplankton production, reaching up to 104% of daily production.[62]

Accounting for all phytoplankton species that we collected, we observed a concave growth−defense trade-off in the Pearl River Estuary (Figure 4). Moreover, we found that the trade-off curves for phytoplankton tended to transition from concave to convex at low and high N:P ratios (Figure S8). However, given the current scarcity of data, the exact nature of how the trade-off curve adjusts to increasing eutrophication requires further investigation. Consistent with model predictions at lower nutrient availability, when $\log_{10}(N:P) < 1.5$ and with phytoplankton species in the estuary exhibiting a concave trade-off, phytoplankton species with both a higher growth rate and a higher defense capacity dominated. These included *S. costatum*, *C. curvisetus*, *C. debilis*, and *C. lorenzianus*. These dominant species had higher nutrient uptake efficiency and defense capabilities than other phytoplankton species (Table S2). Conversely, when $\log_{10}(N:P)$ was greater than 1.5, species tended to exhibit a convex trade-off curve, with divergent survival strategies among the dominant phytoplankton species. Some, like *A. granulata* and *Pediastrum* spp., prioritize high growth rates over defense capabilities, whereas others, such as *N. scintillans*, *Coscinodiscus* spp., and *D. brightwellii*, adopt a lower growth rate so they can enhance their defense mechanisms. Our analysis does not imply that the $\log_{10}(N:P)$ ratio can definitively reveal a tipping point. Accurately identifying tipping points, if they exist, will require more detailed and frequent collection of field data. The emphasis on distinct patterns emerging at different $\log_{10}(N:P)$ ratios is to understand the adaptive strategies of phytoplankton under varying nutrient conditions rather than to establish specific threshold values.

However, our field observations did not fully support that eutrophication favored better-defended species, as we did not observe a clear increase in the dominance of highly defended species or slow-growing species (Figure S11). This discrepancy between the model predictions and field data is not surprising due to the high variability in natural phytoplankton communities and the challenges in accurately quantifying defense traits in the field.[63] Such patterns are more commonly observed in controlled laboratory experiments.[64] More importantly, our data set is limited on both temporal and spatial scales, and conventional sampling methods may underestimate plankton species richness and biomass.[35] Continuous, long-term sampling could capture more details of ecosystem dynamics and better align with model predictions.

4.3. Implications for Adaptive Management of Eutrophic Ecosystems. Our findings highlight the complexity of managing eutrophic ecosystems, particularly through biomanipulation strategies aimed at controlling algal blooms via trophic cascades. While biomanipulation is a widely used approach, its effectiveness can be limited by the slow response of zooplankton populations in reaching densities sufficient to suppress phytoplankton. Furthermore, as eutrophication intensifies, many phytoplankton species develop or more aggressively implement defense mechanisms—such as mucus or toxin production or the formation of large, indigestible colonies—that reduce their vulnerability to zooplankton grazing. These defenses pose significant challenges to biomanipulation efforts, particularly under highly eutrophic conditions where defensively robust phytoplankton species may dominate.

As a result, biomanipulation may be more effective in the early stages of eutrophication, when phytoplankton defenses are weaker and zooplankton can exert greater grazing pressure. However, under severely eutrophic conditions, these defenses may weaken the impact of zooplankton by reducing their ability to control harmful algal blooms. Thus, while biomanipulation seems likely to remain a useful tool, its

https://doi.org/10.1021/acs.est.4c08067
Environ. Sci. Technol. XXXX, XXX, XXX−XXX

effectiveness may diminish as eutrophication progresses.[65] Although recent research has explored the potential of introducing diverse zooplankton species to overcome phytoplankton defenses, the longer-term outcomes of such interventions remain uncertain.[66] This underscores the need for a more comprehensive approach to managing eutrophic ecosystems—one that integrates the eco-evolutionary dynamics of plankton communities and considers both biotic and abiotic factors that influence ecosystem resilience. Continuous monitoring and adaptive management will be crucial for refining these strategies and ensuring they remain effective in complex, nutrient-enriched environments.

■ ASSOCIATED CONTENT

Supporting Information

The Supporting Information is available free of charge at https://pubs.acs.org/doi/10.1021/acs.est.4c08067.

Parameter descriptions and values in the trait-based plankton model; Functional traits of phytoplankton species collected from China's Pearl River Estuary; Statistics for water physicochemical factors in the estuary; Dominance of phytoplankton species collected in the estuary; Diagram of connections between modeling and field observations; Assumed concave and convex growth−defense trade-off curves in the model; Maps of sampling stations; Temporal and spatial distributions of water physicochemical factors in the estuary; Community composition of phytoplankton in the estuary; Biomass dynamics along the eutrophication gradient for the model; Time series of biomass dynamics; Changes in growth−defense trade-offs with increasing N:P ratios; Comparison of *RUE*s related to phytoplankton species growth−defense trade-offs; Relationships between species dominance and *RUE*s; Relative proportion of each species' abundance along the N:P gradient (PDF)

■ AUTHOR INFORMATION

Corresponding Authors

Zhihao Xu − *Guangdong Basic Research Center of Excellence for Ecological Security and Green Development, Guangdong Provincial Key Laboratory of Water Quality Improvement and Ecological Restoration for Watersheds, School of Ecology, Environment and Resources, Guangdong University of Technology, Guangzhou 510006, China; Southern Marine Science and Engineering Guangdong Laboratory (Guangzhou), Guangzhou 511458, China;* orcid.org/0000-0003-3615-6296; Phone: 020-3932-2141; Email: zhihaoxu@gdut.edu.cn; Fax: 020-3932-2141

Zhifeng Yang − *Guangdong Basic Research Center of Excellence for Ecological Security and Green Development, Guangdong Provincial Key Laboratory of Water Quality Improvement and Ecological Restoration for Watersheds, School of Ecology, Environment and Resources, Guangdong University of Technology, Guangzhou 510006, China; Southern Marine Science and Engineering Guangdong Laboratory (Guangzhou), Guangzhou 511458, China*; Phone: 020-3932-2141; Email: zfyang@gdut.edu.cn; Fax: 020-3932-2141

Authors

Xiaoxiao Li − *Guangdong Basic Research Center of Excellence for Ecological Security and Green Development, Guangdong Provincial Key Laboratory of Water Quality Improvement and Ecological Restoration for Watersheds, School of Ecology, Environment and Resources, Guangdong University of Technology, Guangzhou 510006, China; Southern Marine Science and Engineering Guangdong Laboratory (Guangzhou), Guangzhou 511458, China;* orcid.org/0000-0002-4029-2162

Sibo Zhang − *Guangdong Basic Research Center of Excellence for Ecological Security and Green Development, Guangdong Provincial Key Laboratory of Water Quality Improvement and Ecological Restoration for Watersheds, School of Ecology, Environment and Resources, Guangdong University of Technology, Guangzhou 510006, China*

Weilun Gao − *Guangdong Basic Research Center of Excellence for Ecological Security and Green Development, Guangdong Provincial Key Laboratory of Water Quality Improvement and Ecological Restoration for Watersheds, School of Ecology, Environment and Resources, Guangdong University of Technology, Guangzhou 510006, China*

Qian Dong − *Guangdong Basic Research Center of Excellence for Ecological Security and Green Development, Guangdong Provincial Key Laboratory of Water Quality Improvement and Ecological Restoration for Watersheds, School of Ecology, Environment and Resources, Guangdong University of Technology, Guangzhou 510006, China*

Fen Guo − *Guangdong Basic Research Center of Excellence for Ecological Security and Green Development, Guangdong Provincial Key Laboratory of Water Quality Improvement and Ecological Restoration for Watersheds, School of Ecology, Environment and Resources, Guangdong University of Technology, Guangzhou 510006, China*

Zhenchang Zhu − *Guangdong Basic Research Center of Excellence for Ecological Security and Green Development, Guangdong Provincial Key Laboratory of Water Quality Improvement and Ecological Restoration for Watersheds, School of Ecology, Environment and Resources, Guangdong University of Technology, Guangzhou 510006, China; Southern Marine Science and Engineering Guangdong Laboratory (Guangzhou), Guangzhou 511458, China*

Wei Yang − *State Key Laboratory of Water Environment Simulation, School of Environment, Beijing Normal University, Beijing 100875, China*

Complete contact information is available at: https://pubs.acs.org/10.1021/acs.est.4c08067

Author Contributions

X.L., Z.X., and Z.Y. designed the study. X.L. and W.G. conducted the numerical simulations. X.L., S.Z., Q.D., F.G., Z.X., and Z.Z. conducted field observations and collected the data. X.L. conducted the data analyses and wrote the first draft of the manuscript, and W.Y., S.Z., W.G., and Z.X. contributed to the discussion and revisions.

Notes

The authors declare no competing financial interest.

■ ACKNOWLEDGMENTS

This study was financially supported by the National Natural Science Foundation of China (52388101, 52239005, and 52309082), the Program for Guangdong Introducing In-

novative and Entrepreneurial Teams (2019ZT08L213), and the Guangdong Basic and Applied Basic Research Foundation (2022A1515110552).

REFERENCES

(1) Paerl, H. W.; Valdes, L. M.; Peierls, B. L.; Adolf, J. E.; Harding, L. W., Jr Anthropogenic and climatic influences on the eutrophication of large estuarine ecosystems. *Limnol. Oceanogr.* **2006**, *51* (1 part 2), 448−462.
(2) Downing, J. A.; Polasky, S.; Olmstead, S. M.; Newbold, S. C. Protecting local water quality has global benefits. *Nat. Commun.* **2021**, *12*, 2709.
(3) Pannard, A.; Souchu, P.; Chauvin, C.; Delabuis, M.; Gascuel-Odoux, C.; Jeppesen, E.; Le Moal, M.; Ménesguen, A.; Pinay, G.; Rabalais, N. N.; et al. Why are there so many definitions of eutrophication? *Ecol. Monogr.* **2024**, *94* (3), No. e1616.
(4) von Ruckert, G.; Giani, A. Biological interactions in the plankton community of a tropical eutrophic reservoir: Is the phytoplankton controlled by zooplankton? *J. Plankton Res.* **2008**, *30* (10), 1157−1168.
(5) Ger, K. A.; Urrutia-Cordero, P.; Frost, P. C.; Hansson, L. A.; Sarnelle, O.; Wilson, A. E.; Lürling, M. The interaction between cyanobacteria and zooplankton in a more eutrophic world. *Harmful Algae* **2016**, *54*, 128−144.
(6) David, V.; Tortajada, S.; Savoye, N.; Breret, M.; Lachaussée, N.; Philippine, O.; Robin, F.-X.; Dupuy, C. Impact of human activities on the spatio-seasonal dynamics of plankton diversity in drained marshes and consequences on eutrophication. *Water Res.* **2020**, *170*, 115287.
(7) Alves Amorim, C. A.; Do Nascimento Moura, A. Ecological impacts of freshwater algal blooms on water quality, plankton biodiversity, structure, and ecosystem functioning. *Sci. Total Environ.* **2021**, *758*, 143605.
(8) Breton, E.; Christaki, U.; Bonato, S.; Didry, M.; Artigas, L. F. Functional trait variation and nitrogen use efficiency in temperate coastal phytoplankton. *Mar. Ecol.: Prog. Ser.* **2017**, *563*, 35−49.
(9) Hodapp, D.; Hillebrand, H.; Striebel, M. "Unifying" the Concept of Resource Use Efficiency in Ecology. *Front. Ecol. Evol.* **2019**, *6*, 233.
(10) Jin, L.; Chen, H.; Matsuzaki, S. I. S.; Shinohara, R.; Wilkinson, D. M.; Yang, J. Tipping points of nitrogen use efficiency in freshwater phytoplankton along trophic state gradient. *Water Res.* **2023**, *245*, 120639.
(11) Frank, F.; Danger, M.; Hillebrand, H.; Striebel, M. Stoichiometric constraints on phytoplankton resource use efficiency in monocultures and mixtures. *Limnol. Oceanogr.* **2020**, *65* (8), 1734−1746.
(12) Guo, C.; Zhu, M.; Xu, H.; Zhang, Y.; Qin, B.; Zhu, G.; Wang, J. Spatiotemporal dependency of resource use efficiency on phytoplankton diversity in Lake Taihu. *Limnol. Oceanogr.* **2022**, *67* (4), 830−842.
(13) Gerhard, M.; Schlenker, A.; Hillebrand, H.; Striebel, M. Environmental stoichiometry mediates phytoplankton diversity effects on communities' resource use efficiency and biomass. *J. Ecol.* **2022**, *110* (2), 430−442.
(14) Yuan, L. L.; Pollard, A. I. Changes in the relationship between zooplankton and phytoplankton biomasses across a eutrophication gradient. *Limnol. Oceanogr.* **2018**, *63* (6), 2493−2507.
(15) Filstrup, C. T.; Hillebrand, H.; Heathcote, A. J.; Harpole, W. S.; Downing, J. A. Cyanobacteria dominance influences resource use efficiency and community turnover in phytoplankton and zooplankton communities. *Ecol. Lett.* **2014**, *17* (4), 464−474.
(16) Chase, J. M. Food web effects of prey size refugia: Variable interactions and alternative stable equilibria. *Am. Nat.* **1999**, *154* (5), 559−570.
(17) Litchman, E.; Klausmeier, C. A.; Schofield, O. M.; Falkowski, P. G. The role of functional traits and trade-offs in structuring phytoplankton communities: Scaling from cellular to ecosystem level. *Ecol. Lett.* **2007**, *10* (12), 1170−1181.
(18) Barton, A. D.; Pershing, A. J.; Litchman, E.; Record, N. R.; Edwards, K. F.; Finkel, Z. V.; Kiørboe, T.; Ward, B. A. The biogeography of marine plankton traits. *Ecol. Lett.* **2013**, *16* (4), 522−534.
(19) Martini, S.; Larras, F.; Boyé, A.; Faure, E.; Aberle, N.; Archambault, P.; Bacouillard, L.; Beisner, B. E.; Bittner, L.; Castella, E.; Danger, M.; Gauthier, O.; Karp-Boss, L.; Lombard, F.; Maps, F.; Stemmann, L.; Thiébaut, E.; Usseglio-Polatera, P.; Vogt, M.; Laviale, M.; Ayata, S. D. Functional trait-based approaches as a common framework for aquatic ecologists. *Limnol. Oceanogr.* **2021**, *66* (3), 965−994.
(20) Lürling, M. Grazing resistance in phytoplankton. *Hydrobiologia* **2021**, *848* (1), 237−249.
(21) Pančić, M.; Kiørboe, T. Phytoplankton defence mechanisms: Traits and trade-offs. *Biol. Rev.* **2018**, *93* (2), 1269−1303.
(22) Ehrlich, E.; Kath, N. J.; Gaedke, U. The shape of a defense-growth trade-off governs seasonal trait dynamics in natural phytoplankton. *ISME J.* **2020**, *14* (6), 1451−1462.
(23) Brown, E. R.; Kubanek, J. Harmful alga trades off growth and toxicity in response to cues from dead phytoplankton. *Limnol. Oceanogr.* **2020**, *65* (8), 1723−1733.
(24) Grønning, J.; Kiørboe, T. Diatom defence: Grazer induction and cost of shell-thickening. *Funct. Ecol.* **2020**, *34* (9), 1790−1801.
(25) Ehrlich, E.; Becks, L.; Gaedke, U. Trait-fitness relationships determine how trade-off shapes affect species coexistence. *Ecology* **2017**, *98* (12), 3188−3198.
(26) Cadier, M.; Andersen, K. H.; Visser, A. W.; Kiørboe, T. Competition−defense tradeoff increases the diversity of microbial plankton communities and dampens trophic cascades. *Oikos* **2019**, *128* (7), 1027−1040.
(27) Breton, E.; Goberville, E.; Sautour, B.; Ouadi, A.; Skouroliakou, D. I.; Seuront, L.; Beaugrand, G.; Kléparski, L.; Crouvoisier, M.; Pecqueur, D.; Salmeron, C.; Cauvin, A.; Poquet, A.; Garcia, N.; Gohin, F.; Christaki, U. Multiple phytoplankton community responses to environmental change in a temperate coastal system: A trait-based approach. *Front. Mar. Sci.* **2022**, *9*, 914475.
(28) Liu, S. M.; Hong, G.-H.; Zhang, J.; Ye, X. W.; Jiang, X. L. Nutrient budgets for large chinese estuaries. *Biogeosciences* **2009**, *6* (10), 2245−2263.
(29) Huang, W.; Traulsen, A.; Werner, B.; Hiltunen, T.; Becks, L. Dynamical trade-offs arise from antagonistic coevolution and decrease intraspecific diversity. *Nat. Commun.* **2017**, *8* (1), 2059.
(30) Li, X.; Yang, W.; Sun, T.; Gaedke, U. Quantitative food web structure and ecosystem functions in a warm-temperate seagrass bed. *Mar. Biol.* **2021**, *168* (5), 74.
(31) Schneider, F. D.; Brose, U.; Rall, B. C.; Guill, C. Animal diversity and ecosystem functioning in dynamic food webs. *Nat. Commun.* **2016**, *7* (1), 12718.
(32) Niu, L.; Luo, X.; Hu, S.; Liu, F.; Cai, H.; Ren, L.; Ou, S.; Zeng, D.; Yang, Q. Impact of anthropogenic forcing on the environmental controls of phytoplankton dynamics between 1974 and 2017 in the Pearl River Estuary, China. *Ecol. Indic.* **2020**, *116*, 106484.
(33) Koestner, D.; Stramski, D.; Reynolds, R. A. Assessing the effects of particle size and composition on light scattering through measurements of size-fractionated seawater samples. *Limnol. Oceanogr.* **2020**, *65* (1), 173−190.
(34) Zhang, S.; Xia, X.; Xin, Y.; Li, X.; Wang, J.; Yu, L.; Li, C.; McDowell, W. H.; Tan, Q.; Yang, Z. Electrical conductivity as a reliable indicator for assessing land use effects on stream N_2O concentration. *J. Hydrol.* **2023**, *626*, 130253.
(35) Jiang, Z.; Liu, J.; Zhu, X.; Chen, Y.; Chen, Q.; Chen, J. Quantitative comparison of phytoplankton community sampled using net and water collection methods in the Southern Yellow Sea. *Reg. Stud. Mar. Sci.* **2020**, *35*, 101250.
(36) Hillebrand, H.; Dürselen, C.; Kirschtel, D.; Pollingher, U.; Zohary, T. Biovolume calculation for pelagic and benthic microalgae. *J. Phycol.* **1999**, *35* (2), 403−424.
(37) Yang, W.; Li, M.; Sun, T.; Jin, Y. The joint effect of tidal barrier construction and freshwater releases on the macrobenthos community in the northern Yellow River Delta (China). *Ocean Coastal Manage.* **2017**, *136*, 83−94.

https://doi.org/10.1021/acs.est.4c08067
Environ. Sci. Technol. XXXX, XXX, XXX−XXX

(38) Olli, K.; Klais, R.; Tamminen, T. Rehabilitating the cyanobacteria−niche partitioning, resource use efficiency and phytoplankton community structure during diazotrophic cyanobacterial blooms. *J. Ecol.* **2015**, *103* (5), 1153−1164.
(39) Edwards, K. F.; Thomas, M. K.; Klausmeier, C. A.; Litchman, E. Allometric scaling and taxonomic variation in nutrient utilization traits and maximum growth rate of phytoplankton. *Limnol. Oceanogr.* **2012**, *57* (2), 554−566.
(40) Sarthou, G.; Timmermans, K. R.; Blain, S.; Tréguer, P. Growth physiology and fate of diatoms in the ocean: A review. *J. Sea Res.* **2005**, *53*, 25−42.
(41) Edwards, K. F.; Thomas, M. K.; Klausmeier, C. A.; Litchman, E. Phytoplankton growth and the interaction of light and temperature: A synthesis at the species and community level. *Limnol. Oceanogr.* **2016**, *61* (4), 1232−1244.
(42) Sathyendranath, S.; Stuart, V.; Nair, A.; Oka, K.; Nakane, T.; Bouman, H.; Forget, M. H.; Maass, H.; Platt, T. Carbon-to-chlorophyll ratio and growth rate of phytoplankton in the sea. *Mar. Ecol.: Prog. Ser.* **2009**, *383*, 73−84.
(43) Ward, B. A.; Marañón, E.; Sauterey, B.; Rault, J.; Claessen, D. The size dependence of phytoplankton growth rates: A trade-off between nutrient uptake and metabolism. *Am. Nat.* **2017**, *189* (2), 170−177.
(44) Cloern, J. E.; Grenz, C.; Vidergar-Lucas, L. An empirical model of the phytoplankton chlorophyll: Carbon ratio-the conversion factor between productivity and growth rate. *Limnol. Oceanogr.* **1995**, *40* (7), 1313−1321.
(45) Breton, E.; Christaki, U.; Sautour, B.; Demonio, O.; Skouroliakou, D. I.; Beaugrand, G.; Seuront, L.; Kléparski, L.; Poquet, A.; Nowaczyk, A.; Crouvoisier, M.; Ferreira, S.; Pecqueur, D.; Salmeron, C.; Brylinski, J. M.; Lheureux, A.; Goberville, E. Seasonal variations in the biodiversity, ecological strategy, and specialization of diatoms and copepods in a coastal system with *Phaeocystis* blooms: The key role of trait trade-offs. *Front. Mar. Sci.* **2021**, *8*, 656300.
(46) R Core Team. *R: A language and environment for statistical computing*. R Foundation for Statistical Computing: Vienna, Austria, 2022.
(47) Elzhov, T. V.; Mullen, K. M.; Spiess, A. N.; Bolker, B. *minpack.lm: R interface to the Levenberg-Marquardt nonlinear least-squares algorithm found in MINPACK, plus support for bounds: R package version 1.2−3*, Comprehensive R Archive Network, 2023.
(48) Oksanen, J.; Blanchet, F. G.; Kindt, R.; Legendre, P.; Minchin, P. R.; O'Hara, R. B.; Simpson, G. L.; Solymos, P.; Stevens, M. H. H.; Wagner, H. *vegan: Community Ecology Package: R package version 2.6−4*, Comprehensive R Archive Network, 2024.
(49) Papanikolopoulou, L. A.; Smeti, E.; Roelke, D. L.; Dimitrakopoulos, P. G.; Kokkoris, G. D.; Danielidis, D. B.; Spatharis, S. Interplay between r- and k-strategists leads to phytoplankton underyielding under pulsed resource supply. *Oecologia* **2018**, *186* (3), 755−764.
(50) Våge, S.; Storesund, J. E.; Giske, J.; Thingstad, T. F. Optimal defense strategies in an idealized microbial food web under trade-off between competition and defense. *PLoS One* **2014**, *9* (7), No. e101415.
(51) Våge, S.; Bratbak, G.; Egge, J.; Heldal, M.; Larsen, A.; Norland, S.; Lund Paulsen, M.; Pree, B.; Sandaa, R.; Skjoldal, E. F.; Tsagaraki, T. M.; Øvreås, L.; Thingstad, T. F. Simple models combining competition, defence and resource availability have broad implications in pelagic microbial food webs. *Ecol. Lett.* **2018**, *21* (9), 1440−1452.
(52) Rosenzweig, M. L. Paradox of enrichment: Destabilization of exploitation ecosystems in ecological time. *Science* **1971**, *171* (3969), 385−387.
(53) Li, X.; Klauschies, T.; Yang, W.; Yang, Z.; Gaedke, U. Trait adaptation enhances species coexistence and reduces bistability in an intraguild predation module. *Ecol. Evol.* **2023**, *13* (1), No. e9749.
(54) Sailley, S. F.; Polimene, L.; Mitra, A.; Atkinson, A.; Allen, J. I. Impact of zooplankton food selectivity on plankton dynamics and nutrient cycling. *J. Plankton Res.* **2015**, *37* (3), 519−529.
(55) Ke, S.; Zhang, P.; Ou, S.; Zhang, J.; Chen, J.; Zhang, J. Spatiotemporal nutrient patterns, composition, and implications for eutrophication mitigation in the Pearl River Estuary, China. *Estuarine, Coastal Shelf Sci.* **2022**, *266*, 107749.
(56) Serre-Fredj, L.; Chasselin, L.; Jolly, O.; Jacqueline, F.; Claquin, P. Colimitation assessment of phytoplankton growth using a resource use efficiency approach in the Bay of Seine (French-English Channel). *J. Environ. Manage.* **2022**, *306*, 114487.
(57) Lehtinen, S.; Tamminen, T.; Ptacnik, R.; Andersen, T. Phytoplankton species richness, evenness, and production in relation to nutrient availability and imbalance. *Limnol. Oceanogr.* **2017**, *62* (4), 1393−1408.
(58) Ma, M.; Li, J.; Lu, A.; Zhu, P.; Yin, X. Effects of phytoplankton diversity on resource use efficiency in a eutrophic urban river of Northern China. *Front. Environ. Sci.* **2024**, *12*, 1389220.
(59) Huang, H.; Xu, Q.; Song, H.; Chen, N. Genetic diversity and geographical distribution of the red tide species *Coscinodiscus granii* revealed using a high-resolution molecular marker. *Microorganisms* **2022**, *10* (10), 2028.
(60) Chen, Y.-L.; Zhao, L.-S.; Zhou, A.; Shen, S.-L. Evaluation of environmental impact of red tide around Pearl River Estuary, Guangdong, China. *Mar. Environ. Res.* **2023**, *185*, 105892.
(61) Yao, Y.-X.; Chen, N.-S. Biodiversity of phytoplankton and red tide species in the Pearl River Estuary. *Mar. Sci.* **2021**, *45* (9), 75−90. In Chinese with an English abstract
(62) Tan, Y.; Huang, L.; Chen, Q.; Huang, X. Seasonal variation in zooplankton composition and grazing impact on phytoplankton standing stock in the Pearl River Estuary, China. *Cont. Shelf Res.* **2004**, *24* (16), 1949−1968.
(63) Ryderheim, F. *Opening the black box on predator-induced phytoplankton defenses mechanisms, traits, and trade-offs*. Ph.D. Dissertation; Technical University of Denmark: Kongens Lyngby, 2021.
(64) O'Donnell, D. R.; Fey, S. B.; Cottingham, K. L. Nutrient availability influences kairomone-induced defenses in *Scenedesmus acutus* (Chlorophyceae). *J. Plankton Res.* **2013**, *35* (1), 191−200.
(65) Triest, L.; Stiers, I.; Van Onsem, S. Biomanipulation as a nature-based solution to reduce cyanobacterial blooms. *Aquat. Ecol.* **2016**, *50* (3), 461−483.
(66) Zhang, C.; Zhou, Y.; Špoljar, M.; Fressl, J.; Tomljanović, T.; Rama, V.; Kuczyńska-Kippen, N. How can top-down and bottom-up manipulation be used to mitigate eutrophication? mesocosm experiment driven modeling zooplankton seasonal dynamic approach in the trophic cascade. *Water Res.* **2023**, *243*, 120364.

https://doi.org/10.1021/acs.est.4c08067
Environ. Sci. Technol. XXXX, XXX, XXX−XXX